Molecular BioSystems

RSC Publishing

PAPER

View Article Online
View Journal | View Issue

Cite this: *Mol. BioSyst.*, 2013, **9**, 1326

A Boolean view separates platelet activatory and inhibitory signalling as verified by phosphorylation monitoring including threshold behaviour and integrin modulation†

Marcel Mischnik,[a] Desislava Boyanova,‡[b] Katharina Hubertus,‡[c] Jörg Geiger,[c] Nicole Philippi,[d] Marcus Dittrich,[b] Gaby Wangorsch,[b] Jens Timmer*[aef] and Thomas Dandekar*[bg]

Received 21st December 2012,
Accepted 11th February 2013

DOI: 10.1039/c3mb25597b

www.rsc.org/molecularbiosystems

Platelets are critical for haemostasis and blood clotting. However, since under normal circumstances blood should flow without clotting, its function is regulated *via* a complex interplay of activating and inhibiting signal transduction pathways. Understanding this network is crucial for treatment of cardiovascular and bleeding diseases. Detailed protein interaction and phosphorylation data are explored to establish a simplified Boolean model of the central platelet cascades. We implemented the model by means of CellNetAnalyzer and showed how different signalling events coalesce into a fully activated system state. Furthermore, we examined the networks' inherent threshold behaviour using the semi-quantitative modelling software SQUAD. Finally, predictions are verified monitoring phosphorylations which mark different activation phases as modelled. The model can also be applied to simulate different pharmacological conditions as they modify node activity (aspirin, clopidogrel, milrinon, iloprost, combination) and is available for further studies. It agrees well with observations. Activatory pathways are diversified to cope with complex environmental conditions. Platelet activation needs several activation steps to integrate over different network subsets, as they are formed by the interplay of activating kinases, calcium mobilization, and the inhibiting cAMP–PKA system. System stability analysis shows two phases: a sub-threshold behaviour, characterized by integration over different activatory and inhibitory conditions, and a beyond threshold phase, represented by competition and shutting down of counter-regulatory pathways. The integrin network and Akt-protein are critical for stable effector response. Dynamic threshold-analysis reveals a dependency of the relative activating input strength necessary to irreversibly engage the system from the absolute inhibitory signal strength.

Introduction

Platelets represent the key players in mammalian wound healing. Their ability to aggregate and attach to the surrounding tissue of damaged blood vessels is thereby mediated by a complex signal transduction network that comprises both activatory and inhibitory components. Due to its central position for the platelet response to exogenous factors, haemostasis and the fine-tuned

[a] *Institute of Physics, Hermann-Herder-Strasse 3a, 79104 Freiburg, Germany. E-mail: marcel.mischnik@fdm.uni-freiburg.de, jeti@fdm.uni-freiburg.de; Fax: +49 761 203 8541; Tel: +49 761 203 8532*

[b] *Department of Bioinformatics, Biocenter, Am Hubland, 97074 Wuerzburg, Germany. E-mail: desislava.boyanova@uni-wuerzburg.de, gaby.wangorsch@biozentrum.uni-wuerzburg.de, marcus.dittrich@biozentrum.uni-wuerzburg.de, dandekar@biozentrum.uni-wuerzburg.de; Fax: +49 931 888 4552; Tel: +49 931 318 455*

[c] *Institute for Clinical Biochemistry & Pathobiochemistry, Grombühlstraße 12, 97080 Würzburg, Germany. E-mail: k.glasauer@klin-biochem.uni-wuerzburg.de, j.geiger@klin-biochem.uni-wuerzburg.de; Fax: +49 931 201 6 45 001; Tel: +49 931 888 3171*

[d] *Max Planck Institute for Biology of Aging, Gleueler Strasse 50a, 50931 Köln, Germany. E-mail: nicole.philippi@age.mpg.de; Fax: +49 221 4726 345; Tel: +49 221 4726 0*

[e] *Freiburg Institute for Advanced Studies (FRIAS), Albertstrasse 19, 79104 Freiburg, Germany*

[f] *BIOSS Centre for Biological Signalling Studies, Schänzlestrasse 18, 79104 Freiburg, Germany*

[g] *EMBL Heidelberg, Meyerhofstraße 1, 69117 Heidelberg, Germany*

† Electronic supplementary information (ESI) available. See DOI: 10.1039/c3mb25597b

‡ Equally contributing authors.

balance of equilibrated blood flow on one hand, and the lack of profound understanding on the other, the pathway constitutes a convenient target for modelling. Additionally, platelet signalling plays a tremendous role in medicine, as it is directly related to thrombosis, atheriosclerosis and bleeding disorders like von Willebrand disease.[1–3] However, modelling approaches are scarce. Currently, models include the thrombotic process in general,[4] keratinocyte signalling and cell migration,[5] G-protein and calcium responses in activated platelets[6] and cAMP–cGMP networks.[7] The crucial signalling events leading to irreversible aggregation and cytoskeleton based shape change nonetheless remain unclear. A broad comprehension of the underlying dynamical processes is of high medical importance, since severe diseases like cardiovascular or bleeding disorders are caused to a great extent by inappropriate platelet function.

Boolean models

Many currently available biological models are developed on the basis of ordinary differential equations (ODEs). The power of ODE-based approaches regarding dynamic simulations and systems analysis is beyond question. Anyway, in the case of larger networks, the use of ODE models is confined, due to the limited amount of experimental measurements. Parameter estimation methods for ODE models largely depend on the disposability of time-resolved quantitative data, which is still a bottleneck in systems biology.

In this study, we present a Boolean network of platelet signal transduction. Boolean or logical networks are well suited to reproduce the qualitative behaviour of extensive networks even with a limited amount of experimental data. Boolean logic is the algebra of two values, *e.g.* ''1 and 0'' or ''true and false'' or ''on and off'', and was first shown to be applicable to electrical relay circuits, but then used in different areas of cellular signalling.[8–13]

Interactome overview and identification of key nodes

We focus here on platelet activation for thrombosis and haemostasis and its interplay with inhibitory pathways.

Platelets possess a bulk of surface receptors for both activating and inhibiting ligands. The combination of activated receptors at a given time point determines the system's behaviour. Concerning the activatory fraction, receptors of the P2 type are of particular importance. Three P2 receptors can be found on platelets: two (P2Y1 and P2Y12) are receptors for adenosine diphosphate (ADP), and one (P2X1) is a receptor for adenosine triphosphate (ATP).[14] ADP acts as an autocrine and paracrine ligand, which is produced and released upon platelet binding to an exposed extracellular matrix of damaged blood vessels. The P2Y1 receptor, which is coupled to Gq and phospholipase C-b, is responsible for mobilization of ionized calcium from internal stores and mediates the ADP-induced platelet shape change and initial wave of rapidly reversible aggregation.[15] The other ADP receptor, P2Y12, is negatively coupled to adenylyl cyclase through Gi and mediates a progressive and sustained ADP-induced aggregation.[15,16] In addition, this receptor plays an important role in the potentiation of platelet secretion induced by several platelet agonists. The combined action of P2Y1 and P2Y12 is necessary for the full platelet aggregation response to ADP.[17] The inhibitory pathways involve adenylyl cyclase stimulated through adrenaline and prostaglandin receptors (activated *via* prostaglandin E1, D2 and I2), guanylyl cyclase which is directly activated by nitric oxide and ectonucleotidases.

Downstream of the receptor level, a complex network of kinases, executing proteins and small molecules, can be observed that includes both positive and negative feedback loops as well as auto- and paracrine signalling (Fig. 1). Key activating cascades and modulatory inhibitory cyclic nucleotide pathways are shown. Fig. 1 shows that in addition there are a number of further interactions. In fact, this can be iterated to derive a rather complex ''PlateletWeb'' of all protein–protein interactions within the platelet.[18] For model establishment, it is instead important to select here and focus on key signal interactions in platelet activation and inhibition so that these responses can be reliably predicted and semi-quantitatively modelled. After activation of the P2 receptors (P2Y1 and P2Y12), the signal is transduced to the G-proteins (the Gq- and the inhibitory Gi protein, respectively), which then cause further signalling. P2Y1 acts by activation of PLC-beta and subsequent mobilization of intracellular calcium and P2Y12 by inhibition of adenylyl cyclase through the Gi-alpha subunit and activation of PI3-kinase through the beta-gamma subunit. Central kinases involved in downstream signalling such as the activatory kinases Src and PKC and the inhibitory kinase PKA can be further analysed in a network context along with their phosphorylated substrates. The downstream effects of platelet activation such as shape change, triggered by the activation of integrins, are also included in the model. Phosphorylations are extracted from the literature and additional linking proteins are added to maintain the network integrity.

For each subpart of the network, a set of key-nodes was considered that govern the overall-behaviour of the respective subpart, and that are highly connected to other network partitions. Concerning the activating nodule, this applies to phospholipase C beta and the small GTPase Rap1. Phospholipase C beta gathers signals from all stimulating receptors and produces a second messenger response represented by inositol-trisphosphate (IP_3) and diacylglycerol (DAG).[19,20] Rap1 integrates the activating and inhibiting signals of the respective kinases and initiates aggregation *via* the engagement of talin, which transfers the signal to integrin $\alpha 2b\beta 3$. Of high importance in this context is also the Akt kinase, which receives signals from PI3-kinase and acts directly upon integrin $\alpha 2b\beta 3$, the final executor of the activating partition.[21]

In terms of the inhibiting pathway, protein kinase A (PKA) and its activating second messenger cAMP have to be designated. Cyclic adenosine monophosphate (cAMP) is produced upon stimulation of prostaglandin-receptors (IP1, DP2, EP2, EP4) and exerts its main effects by binding to the regulatory subunits of type I and type II PKA. The catalytic subunits of the kinases then dissociate and phosphorylate selected serine and threonine residues on target proteins that prevent or reverse platelet activation.[22] These include other kinases (Src),

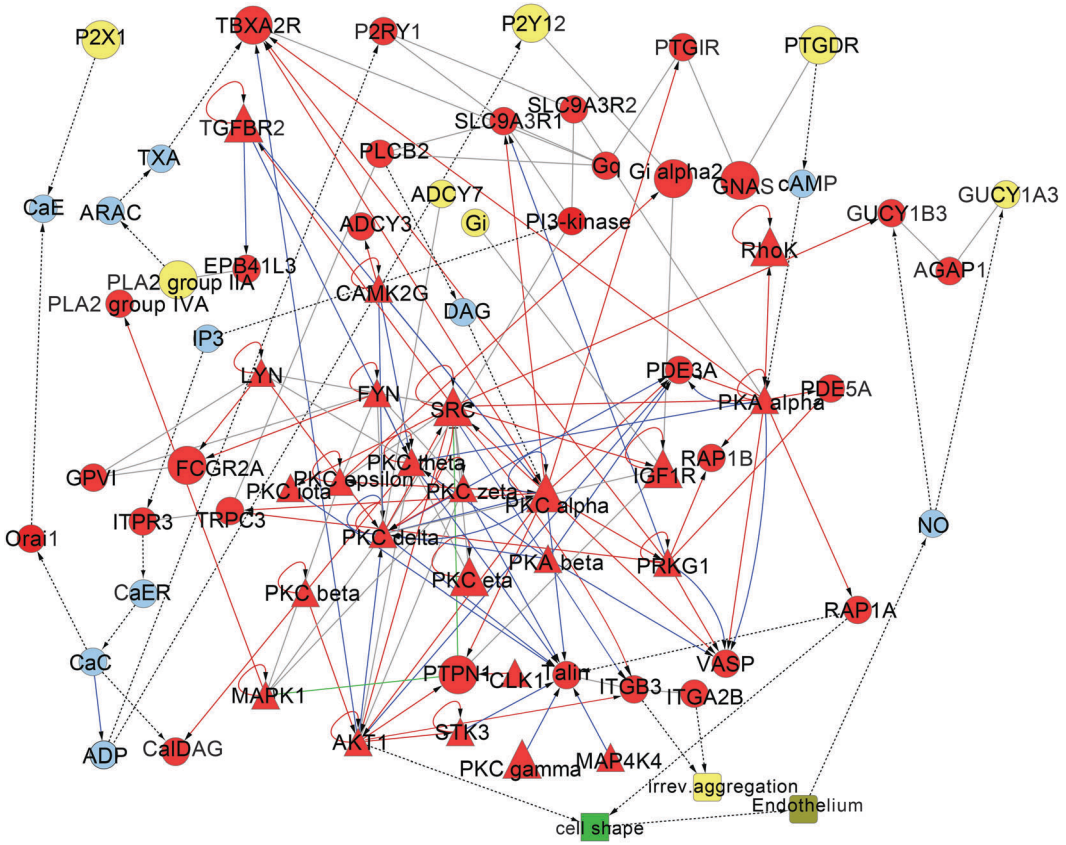

Fig. 1 Key activating platelet cascades and modulatory inhibitory cyclic nucleotide pathways. The figure illustrates detailed data available for modelling of key-nodes considered. Involved in the different activatory and inhibitory platelet receptors are PGI signalling, P2Y12 receptor, P2X1 receptor as well as various interacting proteins. Highly connected activating modules involve phospholipase C beta and the small GTPase Rap1. Rap1 integrates the activating and inhibiting signals of the respective kinases and initiates aggregation *via* the engagement of talin which transfers this and the Akt kinase signal to integrin α2bβ3. Cytoscape visualizes the complexity of the involved pathways. All shown interactions (grey lines), site-specific phosphorylation events (red arrows with labeled sites) and dephosphorylation events (green lines) are extracted from literature studies based on the PlateletWeb knowledge base. Kinase predictions (blue lines) were additionally added to the model. Kinases are presented as triangles and proteins as circles. Phosphorylated proteins are depicted in red. Additional proteins were included for maintaining the network structure and improving the visualization of the signal flow (for example G-proteins). Metabolites and small molecules (NO, ADP, Ca^{2+}, IP_3, DAG, cAMP, thromboxane, arachidonic acid) are presented in light blue circles. A large size of the nodes denotes that the gene coding for the protein is associated with a genetic disease.

receptors (IP3R) and proteins linked to cytoskeletal organization like the vasodilator protein VASP.[23–25] cAMP levels are tightly regulated by means of several negative and positive feedback loops, comprising directly or indirectly activated phosphodiesterases and the G_i-protein coupled ADP receptor P2Y12.[26–28]

Another important network node is the intracellular calcium concentration, also acting as a second messenger. When raised over a distinctive threshold, a cytoskeletal shape change is induced, enabling the platelet to adhere to and migrate towards damaged tissue. Calcium is stored in the dense tubular system and dense granules and released upon activation of the IP_3-receptor. Elevated cytosolic calcium concentrations in turn enable plasma-membrane located calcium release activating calcium-channels ORAI1 and TRPC6, which mediate the store-operated-calcium-entry (SOCE).[29] Another factor increasing cytosolic calcium levels and hence platelet activation is the binding of ATP to its plasma-membrane receptor P2X1, which represents a ligand-gated ion channel for calcium.[30]

In summary, we present here the fast logic of platelet receptor activation in a simplified model, and demonstrate how the receptor signals converge to process activation information. We show furthermore different steps involved in full platelet activation and examine potential thresholds. These findings are validated by experimental results.

Materials and methods

Model implementation

On the basis of literature data, we constructed a comprehensive network map of the involved signalling pathways. Table S1 (ESI†) gives justifications for the different nodes and interactions modelled. The reference numbering of Table S1 (ESI†) is exactly as cited in the manuscript reference list and a higher reference number (ref. 69–87) refers exclusively to Table S1 (ESI†). As an abstraction based on Table S1 (ESI†) we derived a Boolean model. CellNetAnalyzer served for implementation.[31,32] Manual analysis and the identification of network wide dependencies become error-prone for large logical networks. Therefore, construction and analysis of the logical interaction hypergraph model is achieved more reliably in this

study using CNA.[31] ESI† gives full detail: setting up the CNA simulation, details about Boolean operators and applied logical rules, literature-justifications for all interactions and experimental data including drug intervention points.

The logical steady state (LSS) of variables with a unique LSS for a given input setting is determined. For the computation of LSSs the software tool CellNetAnalyzer (CNA) is used, which is available as a Matlab toolbox. The propagation of signals through the network is thereby calculated by iterative derivation of partial LSSs for smaller subnets based on already identified partial LSS until no further ones can be found.[32] The initial condition assumed is equilibrium (all node states equal 0) and no external activating or inhibiting signal. Then specific activation or inhibition is modelled by activating or inhibiting the specific input node. Nodes can assume infinite discrete conditions in addition to the fundamental states 0 and 1. For each of these conditions, an assignment rule can be set, which has to be fulfilled in order to make the species reach the respective level. Due to the nature of the applied steady-state calculation, oscillations in system-states can be neglected.

Additionally, the definition of phases is possible, according to which a certain edge (defined by a rule) only becomes active, if the system is set to a previously defined phase. All edges that are allocated to a higher phase are then excluded from the LSS-calculation.

Detailed information about Boolean operators can be found in the ESI.†

Dynamic simulations using SQUAD

SQUAD represents a qualitative modelling tool. It enables dynamical modelling in a data-free three-step manner.[33] First, it uses Boolean algorithms to identify all stable steady states of the network. Second, the program converts the network into a continuous dynamical system, in the form of a set of ODEs, and uses the steady states found in the discrete model as a guide to localize the stable steady states in the continuous model. And third, SQUAD allows the user to perform dynamic simulations, which may include perturbations, to assess the behaviour of the network and identify the roles of specific nodes within the network. Regarding our platelet system, SQUAD was used to gain information about the network's inherent steady-states and its threshold behaviour (Fig. 3).

Incorporation of experimental data

Experimental data measured for this study involved VASP and cAMP time-courses after stimulation with different ligands, measurements of intracellular calcium levels and several protein phosphorylations and their intensity. Furthermore, we considered experimental data from available literature such as the non-existence of a platelet-owned NO-synthase. Such information is central to delineate the correct model topology.

Platelet preparation

Blood was obtained after informed consent from healthy volunteers who had not received any medical treatment during the prior two weeks according to our institutional guidelines and the Declaration of Helsinki. Our studies with human platelets were approved and reconfirmed (September 24, 2008) by the local ethics committee of the University of Würzburg (studies 67/92 and 114/04). Platelets were used as washed platelets (WP) resuspended in HEPES buffer (145 mM NaCl; 5 mM KCl, 1 mM $MgCl_2$; 10 mM HEPES; 10 mM D-glucose, pH 7.4), depending on the assay applied, and prepared from whole human blood as described elsewhere[27] with modifications to avoid contamination by other cells. Whole human blood was obtained from healthy volunteers who had not taken any medication affecting platelet function within 2 weeks prior to the experiment after informed consent according to the declaration of Helsinki and our institutional guidelines and as approved by the local ethics committee. The blood was drawn by venipuncture and collected in 1/5 volume of citrate buffer (120 mM NaCl, 20 mM sodium citrate, 4 mM KCl, 1.5 mM citric acid, 30 mM D-glucose, pH = 6.5) and centrifuged at 300× *g* for 20 minutes at 20 °C to obtain platelet rich plasma (PRP). For the preparation of washed platelets the PRP was diluted 1 : 1 with HEPES/citrate buffer, apyrase (2 U ml^{-1}) was added and centrifuged again at 200× *g* for 10 min at 20 °C. The pellet was discarded and the supernatant was centrifuged at 380× *g* for 10 minutes. The resulting pellet was resuspended in HEPES/citrate, left resting for 5 minutes and centrifuged again at 380× *g* for 10 minutes. The platelet pellet was resuspended in HEPES buffer to a cell density of 3×10^8 platelets per ml and apyrase (0.1 U ml^{-1}) was added. Washed platelets were used in 200 µl portions. The samples were incubated with the reagents in the water bath at 37 °C as indicated, stopped and treated appropriately for the respective analyte. The reagents were dissolved in HEPES buffer unless otherwise stated.

Calcium measurement

Intracellular calcium regulation was determined fluorometrically with the fluorescent indicator Fura-2 as described previously.[34] Briefly, platelet rich plasma was incubated with 4 µM Fura-2/AM (di-methyl sulfoxide (DMSO) 1% v/v) for 45 minutes, centrifuged at 350× *g* and the resulting platelet pellet resuspended in HEPES buffer (150 mM NaCl, 5 mM KCl, 1 mM $MgCl_2$, 10 mM D-glucose, 10 mM HEPES, pH 7.4). The calcium transients were observed in a Perkin-Elmer LS50 luminescence spectrophotometer at an excitation wavelength of 340 nm and an emission wavelength of 510 nm. Data were recorded as relative changes in the Fura-2 fluorescence signal.

cAMP detection

Cyclic adenosine 5′ monophosphate (cAMP) determination was carried out as described.[27] In brief, platelets were lysed with the original volume of 70% (v/v) ice cold ethanol and kept on ice for 30 minutes. The precipitate was removed by centrifugation for 10 minutes at 10 000× *g* and 4 °C and washed again with the same volume of 70% (v/v) ethanol. The ethanol extracts were combined and dried under vacuum. The dried samples were dissolved in 200 µl of the assay buffer supplied with the assay and acetylated to increase assay sensitivity as described.[27] The samples were measured in a Wallac Victor 1420 (Perkin-Elmer)

plate reader at 405 nm. Sample readings below 30% or above 70% %B/B0 are off the dynamic range of the assay and were repeated with an appropriate dilution of the sample.

VASP assay

VASP phosphorylation is a highly sensitive indicator for platelet cAMP regulation. We determined VASP phosphorylation in a solid-phase assay by VASP binding on a zyxin matrix. The zyxin matrix pVASP assay was carried out as described elsewhere.[27] Platelet samples (200 μl each) were lysed by addition of an equal volume of ice cold lysis buffer (20 mM Tris–HCl, 150 mM NaCl, 1 mM EDTA, 1 mM EGTA, 1% Triton X-100, 0.5% NP-40, 10 mM β-glycerolphosphate, 10 mM NaF, pH = 7.4) and thorough mixing on a vortex mixer. The samples were diluted with PBS buffer by a 1 : 10 ratio. Each sample was measured in triplicate for the VASP phospho-Ser157 antibody (5C6) and total VASP antibody (IE273). As control for background and non-specific binding 5% bovine serum albumin (BSA) dissolved in lysis buffer was used. 100 μl sample per well of the zyxin coated microtiter plate were incubated for 1 h at room temperature under shaking and washed three times with 300 μl per well PBS-T (0.1% Tween20 supplemented PBS), 1 h incubated with the primary antibodies, washed 3 times with PBS-T, the secondary antibody (horse radish peroxidase coupled goat anti-mouse IgG) added, incubated and washed as mentioned above. The detection reagent ABTS was added, incubated for 20 minutes at room temperature under shaking and the absorbance of the samples was measured in the microtiter plates using a Wallac Victor 1420 (Perkin-Elmer) plate reader at 405 nm each for 1 second. From the absorbance of each sample the absorbance of the background control sample for the respective antibody was subtracted, and the resulting data multiplied with the dilution factor. From the values obtained with the phosphospecific and the total VASP antibodies the phospho-VASP/VASP ratio was calculated.

Results and discussion

A standard scenario of activation

In the following, we describe and analyse in detail one standard course of model behaviour. However, the Boolean model allows us to also analyse completely different input combinations and sequences (*e.g.* different inhibitory signalling sequences). Literature confirmations of all stated interactions as well as the applied logical assignment rules can be found in the ESI.† We used the platelet knowledgebase and the literature sources from the Introduction, further key references incorporated into the model are given in the following. The main task involved selection of the modelled signalling nodes and their type of interaction so that activation and inhibition of the platelet could be reliably modelled. Several generations of model setup, performance monitoring and expert curation of the network structure followed before the presented model could be established. Furthermore, a large set of data available (see Validation and experimental verification section) in particular regarding phosphorylation states of kinases and substrates was kept aside and only used in the final step, validation of the established model.

We start from a point in phase space, where the activation levels of all pathway constituents are 0. Upon stimulation of the platelet *via* the strong activator GPVI, a cascade of kinases, including PKC, Akt and Src is engaged, which leads initially to a rearrangement of the cytoskeleton (shape change) and formation of unstable aggregates (reversible aggregation) (Fig. 2). In a first step, membrane-bound phospholipase C beta is activated *via* a G-protein (not included), which triggers the production of the second messengers IP_3 and DAG. The latter one remains at the plasma membrane acting as a potent activator of protein kinase C (PKC).[35] IP_3 diffuses through the cytoplasm, subsequently binding to IP_3-receptors at platelet organelle membranes, which entails the release of calcium ions from intracellular storage pools.[36] This results in a transition of the oblate discoid to a spherical shape of the platelet followed by the formation of cell membrane protrusions (pseudopodia). In addition, PKC-activity is further enhanced and the guanine nucleotide exchange factor CalDAG-GEFI activated.[37] The latter directly activates Rap1, thereby passing the signal *via* talin to integrin $\alpha2b\beta3$ and switching integrin to an active state with an exposed fibrinogen binding site. Activated PKC phosphorylates Src kinase,[38] which also represents a target for PKA phosphorylation.[39] Depending on which input dominates, Src either transmits the signal to the Akt kinase[40] or remains in an inactive state. Akt kinase finally is a direct effector of integrin $\alpha2b\beta3$,[41] boosting the platelet's activation state to a higher level. A fourth important effect of increased intracellular calcium concentration is the fusion of platelet granules with the plasma membrane, thereby releasing small molecules like ATP, ADP or serotonin and procoagulatory proteins into the extracellular space.[42] ADP subsequently binds to its receptors P2Y1 and P2Y12, resulting in a further amplification of the kinase cascade, and an inhibition of cAMP-production by means of P2Y12 on the other hand.[43] Thus, the inhibiting part of the signalling network is suppressed, which additionally increases the platelet's activation state. Finally emptying of calcium stores elicits a secondary calcium entry by means of ORAI1 and TRPC channels. The standard scenario assumes the ATP-receptor and calcium-channel P2X1 to be engaged along with the two ADP receptors. The activated system is stabilised by means of a positive feedback loop from the activated integrin back to the inner side of the plasma membrane, by which PLA2 and COX1 are activated. As a result, thromboxane A2 is synthesized and released, acting as a ligand for platelet thromboxane receptors, thus increasing the pathway activity to the highest extent. Thus, the network behaviour switches from reversible to irreversible aggregation.

System phases and integrin output

The standard activation scenario involves four phases. As the activation signal travels in the model, the CellNetAnalyzer based simulation (see Materials and methods) monitors how more nodes and regions become activated (non-zero activation; maximum activation level is 5) and four phases distinguish how further regions become activated and signal strength increases in regions already activated. The phases were introduced both

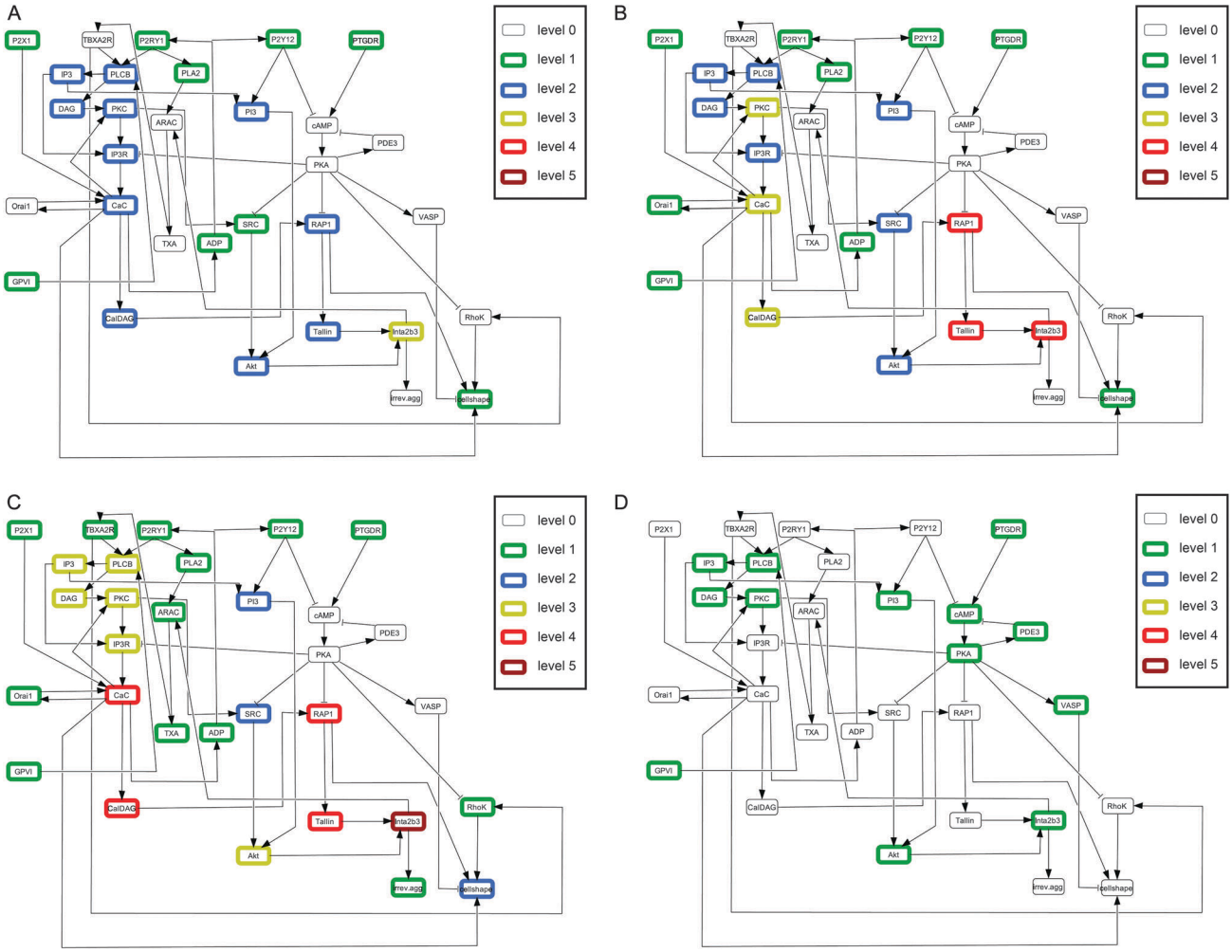

Fig. 2 (A–D) Different system states after logical steady state computation. Successively added network functions coalesce into a fully activated system. (A) t0. Included are solely reactions evoked by pure GPVI signalling. (B) t1. Effects from autocrine ADP signalling are added. (C) t2. Signalling complemented by store-operated-calcium-entry (SOCE). (D) t3. Addition of the positive feedback loop established by integrin signalling results in a maximally engaged system. Activation levels are colour-coded (0 to 5; CellNetAnalyzer simulation).

on the basis of literature, and according to emergent features of the model, which require the coalescence of different network parts to fully activate single nodes. We thus came from two sides: clear evidence from publications as well as system properties of the model, *e.g.* if there are no different activation strengths, there is no full activation, no threshold behaviour and similar features, all of which are also features of real platelets *in vivo.* ESI† shows in detail, which edges operate in which phases.

The first activation phase (Fig. 2A) comprises the prostaglandin/cAMP pathway, the initial binding of a strong activator to its receptor (GPVI) and the subsequent signal transduction cascade that activates integrin α2bβ3 to level 1 or 2 (if inhibitory signals are absent). In the second step (Fig. 2B), ADP is released as a result of a calcium transient and enhances the signalling cascade. Thereby, the integrin α2bβ3 activation state is raised to level 2 or 3. The third step (Fig. 2C) involves SOCE, mediated by the release of calcium from intracellular calcium storage pools and a subsequent activation of the calcium channel ORAI1. Integrin α2bβ3 reaches level 4. In the last phase (Fig. 2D), a positive feedback loop from level 4 integrin activates the network and intercalates the synthesis of thromboxane B2 from arachidonic acid, catalysed by cyclooxygenase. Thus, integrin achieves activation level 5 and the platelets aggregate irreversibly. Logical connections are not modified during the simulation and to be active a signal has to be received at the respective node. All logical rules and system phases in which they become active are now specified in Table S2 in the ESI.† The phases activate different subparts of the network. In the early phases 0, 1 and 2, the system changes occur within a few seconds. Such rapid kinetics are challenging both in terms of time-resolved measuring and dynamical modelling. Though Boolean modelling delivers a highly simplified view of the respective system, it has the advantage that no detailed kinetics are necessary, and that fast changes can be monitored as different system states in the separate phases. Furthermore, the respective time phases are directly verifiable by different phosphorylations and phosphorylation monitoring (see functional data below).

General system features

The fine-tuned balance between thrombosis and haemostasis is critical to understand signalling in platelets. In general, we found two steps of activation in the model: the first step is characterized by a sub-threshold behaviour that allows rapid comparison and integration between different receptor signals and stimuli, both activatory and inhibitory. In this context, several distinct sequences between the respective stimuli are possible. In a second step, after a specific signalling decision is made (specific system thresholds were crossed), all other pathways are competitively closed down.

Steady state analysis

Steady state and threshold analysis were performed using the software SQUAD. Two distinct steady states could be observed: a general off-state where all components have an activation level of 0, and an on-state, depicting the fully-excited system, stabilized by the positive feedback loops. Here, all network nodes exhibit an activation-level of 1 (arbitrary units), except for those involved in the inhibitory cAMP-pathway (cAMP, PKA, VASP and PDE3).

Threshold analysis

Threshold analysis was started from the general off-state. In the first scenario, the system is excited *via* a GPVI-pulse with strength 1. Activating the downstream components, the signal is transduced to integrin, which leads to aggregation and shape change. Akt kinase activity goes through an initial increase, but diminishes as GPVI-input and thus Src signalling flattens. Due to the positive feedback, its activity increases again, finally leading to the fully activated enzyme (Fig. 3A). If the decaying GPVI-input is replaced by a constant one, the system straightly goes to the on-state. In the second scenario, the GPVI-pulse is accompanied by a PTGDR input of strength 0.5. Akt and calcium are slightly mobilized, but due to the inhibitory effect of PKA, the system returns to its deactivated state (Fig. 3B). Constant inputs in place of pulsed ones render the system to be oscillating (data not shown). If a PTGDR input of the same strength is combined with a stronger GPVI-pulse (Fig. 3C), the system transgresses the dynamical threshold, and ends up in its fully activated state. The minimal GPVI-value that leads to threshold-transgression, given a PTGDR-value of 0.5, equals 1.168 (Fig. 3D). Here, the system alternates between both steady-states, as integration of the competing inputs proceeds, but finally ends up in state 2. Akt kinase for instance receives the activating signal from the GPVI analogue, Fig. 3A, but since Src kinase also sustains inhibition from PKA, its activity shortly tumbles until full mobilization is achieved. Calcium dynamics occur as a result of coalescing IP_3, ORAI1 and PKA effects and are reproduced by measurements (Fig. 5A). Table 1 shows different combinations of inhibitory input strength, and the necessary activating input value to exceed the threshold (arbitrary units in terms of full ($\geq$1.0) or no (0.0) activation). After transgressing the threshold, platelet activation is committed and proceeds to full activation. In fact, such sub-threshold behaviour for a combination of activatory and inhibitory inputs has been noted for the platelet inhibitory cyclic nucleotide pathway before.[44] The relative activating strength ($GPVI_{thre}$/PTGDR), that transgresses the threshold, decreases with elevating PTGDR inputs. Thus, the system adapts for higher prostaglandin-concentrations by increasing its sensitivity for activators like vWF and collagen, and thereby commits thrombocyte-dependent active processes such as wound healing even if subsequently blood prostaglandin-levels are higher in later time points. Different efficiencies for various combinations of agonists and antagonists can thus be compared in the model leading to different responses depending on over- or sub-threshold behavior. As a concrete application example for such modelling, different prostanoid receptor antagonists have been experimentally compared for therapeutic strategies regarding prostanoid receptor agonists[45] and various studies compared antithrombotic effects such as the antithrombotic effect of the soluble GPVI dimer compared with anti-GPVI antibodies.[46]

Feedback loops and overall system behaviour

Following a GPVI trigger, the model reacts with activating the necessary signalling components for aggregation and shape change. For an irreversible activation it is however required to increase the input strength by autocrine messengers like ADP and thromboxane. The impact of ADP comes into play after a short time-delay (time-level 2), since migration of cytosolic vesicles to the plasma membrane is realized by time-consuming cytoskeletal transport. This feedback loop needs to be accompanied by at least one other positive loop in the absence of an inhibitory prostaglandin input in order to make the platelet aggregate irreversibly, namely either calcium SOCE or autocrine thromboxane production. With an inhibitory cAMP signal, the system has to be stabilized by outside-in signalling of activated integrin $\alpha 2b\beta 3$ and subsequent release of thromboxane for threshold transgression. Several subnetworks increase system stability as well as render the platelet susceptible to versatile inputs. Consequently, platelet activation needs several activation steps to integrate over different receptors. If an excitatory signal is not sufficient to make a thrombocyte release its autocrine messengers, a possible paracrine effect evoked by neighbouring cells can still elicit an irreversible activation. Engagement of all three loops leads to platelet aggregation regardless of cAMP levels. In a scenario where the only input affecting the system is a prostaglandin ligand, all components except for PTGDR, cAMP, PKA and VASP are 0. This represents the inhibited system state.

Modeling the effects of component disruptions and pharmacological modulation

Inherent to mathematical models is the opportunity to simulate easily the effects of knock-out mutations or medical drugs. The impact of the antithrombotic drug clopidogrel on thrombocyte signal transduction is of high medical relevance.[47] Widely applied in heart disease treatment, clopidogrel represents an antagonist of the ADP receptor P2Y12, which exerts both a crucial activating impact on the platelet kinase machinery and

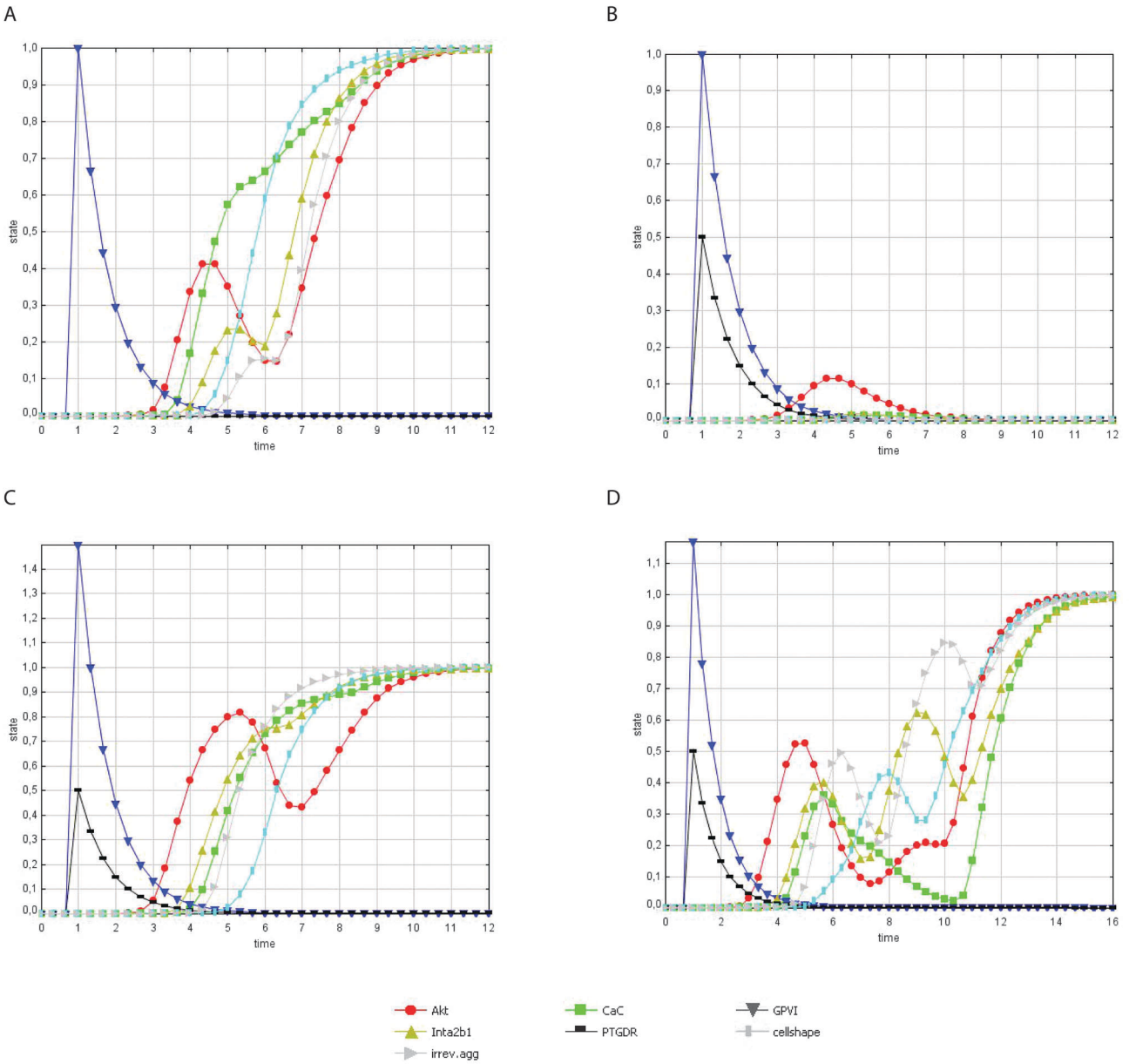

Fig. 3 (A–D) Threshold analysis by dynamical simulation. (A) GPVI input with strength 1. System is in on-state. (B) Combined GPVI input with strength 1 and PTGDR input with strength 0.5: system is in off-state. (C) Combined GPVI input with strength 1.5 and PTGDR input with strength 0.5: system is in off-state. (D) Combined GPVI input with strength 1.2 and PTGDR input with strength 0.5: system behavior in the vicinity of threshold.

Table 1 GPVI-values necessary to exceed the activation threshold

Inhibitory input PTGDR (a.u.)	$GPVI_{thre}$ (a.u.)	Relative activating strength ($GPVI_{thre}$/PTGDR)
0.25	0.946	3.784
0.5	1.168	2.336
0.75	1.456	1.941
1.0	1.625	1.625

a profound closing down of cAMP production, thereby tempering the inhibitory subnetwork. In our model, P2Y12 is positively connected to PI3-kinase, and negatively to cAMP. Blocking of P2Y12 results in a seriously weaker activation of all prothrombotic kinases after a vWF input, and a higher PKA activity, due to increased cAMP values, which is compatible with current experimental data.[48,49] PI3-, Src- and Akt kinase do not exceed an activation-level of 1 even in the last phase. However, since depletion of intracellular calcium-pools and SOCE can still occur, cytoskeletal shape change is engaged in this scenario and integrin α2bβ3 reaches a level of 2. A blocking of either Akt kinase or CalDAG on the other hand leads to a mere integrin-level of 1. Combined blocking of Akt kinase and CalDAG prohibits even the slightest integrin activation. Experimental data support this direction of signal processing (Table 2; Fig. 4A–D, further data available in Table S3, ESI†).

Table 2 Kinase-activation according to system-phases[a]

Kinase	Phase 0	Phase 1	Phase 2	Phase 3
PKA	1	0	0	0
PKC	1	2	3	3
Akt	1	2	2	3
Src	0	1	1	1
PI3	1	2	2	2
Graphical summary of experimental data from the literature	Fig. 4A (*e.g.* kinases shown as triangles: Akt, PI3 and phosphorylated PKA active)	Fig. 4B (*e.g.* Src kinase also phosphorylated)	Fig. 4C (*e.g.* strong activation of PKC)	Fig. 4D (*e.g.* PKC strongly active, integrin network active (red circles)

[a] Figures representing the graphical view of these phases are shown in the last row. The activation state of platelet kinases is shown in the table above with the maximum activation state depicted with the number 3. PKA is active during phase 0, which is in agreement with experimental data projected on the signalling network as shown in Fig. 4A. PKC is mainly active in phases 2 and 3 (Fig. 4C and D). Akt kinase becomes activated during phase 1 (Fig. 4B) with strong activation in phase 3 (Fig. 4D), while Src kinase is moderately active during phases 1, 2 and 3 (Fig. 4B–D). The activation state of PI3-kinase is maintained throughout all phases, but increases from phase 0 to phase 1 (Fig. 4B).

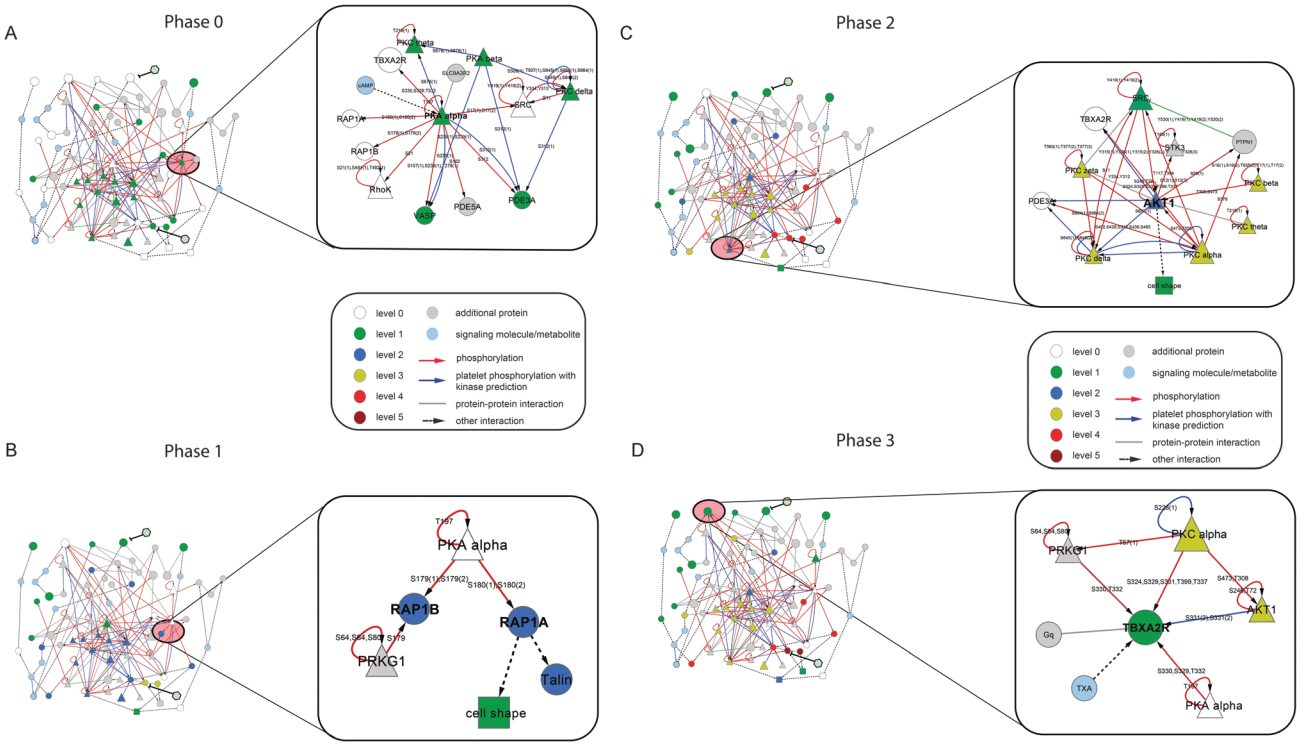

Fig. 4 (A–D) Validation: PlateletWeb. ADP signalling networks visualized and colored according to the Boolean model phases ((A) phase 0; (B) phase 1; (C) phase 2; (D) phase 3). Key phosphorylation events according to experimental data are shown resolved next to each network (phase 0: subnetwork around PKAα, phase 1: around Rap 1a/b; phase 2: around Akt1; phase 3: around TbxA2R). The Boolean model (Fig. 2) is validated here by data on phosphorylation, kinases and substrates not used for setting up the Boolean model but according to experimental data available downloaded from the PlateletWeb knowledgebase (Boyanova *et al.*, 2012). All shown interactions (grey lines), site-specific phosphorylation events (red arrows with labelled sites) and dephosphorylation events (green lines) are extracted from literature studies based on the PlateletWeb knowledge base. Kinase predictions (blue lines) were additionally considered. Kinases are presented as triangles and proteins as circles. High resolution pictures of the phases including the complete network with protein names are given in ESI,† its part B gives experimental data references for all interactions and protein nodes modelled. The rest of the proteins were added for maintaining the network structure and improving the visualization of the signal flow (for example G-proteins). These were not part of the Boolean model. Metabolites and small molecules such as NO and Ca^{2+} are presented in light blue circles. A large size of the nodes denotes that the gene coding for the protein is associated with a genetic disease. Two important inhibitors of platelet function were additionally included: the P2RY12 receptor inhibitor ticagrelor and the ITGB3 inhibitor abciximab. Full detail in supplemental figures phase 0–1 and phase 2–3.

These examples show that direct applications of our model are prediction and interpretation of genetic modifications and therapeutic interventions, for instance in platelet hyper-reactivity. For these functions, nodes such as PEAR1, VAV3 and ITPR1[50] have been shown to be implied and the subsequent nodes Rap1, Talin and integrin from our model should be considered. Changing the Rap1/Talin input to activatory induces also hyper reactivity in our model.

Validation and experimental verification

After establishing the model, we validated it by different experimental data: we show that phosphorylation sites actually

measured using mass-spectrometry agree with the different activation steps investigated. This applies also for an inhibitory scenario (*e.g.* Iloprost stimulation) and substrates (data not shown).

Furthermore, verified kinase data were obtained from the PlateletWeb knowledgebase according to published data and agree well with key activation steps postulated by the model. To complement these data, we furthermore investigate cAMP levels after Iloprost stimulation and compare them with the model as well as direct VASP phosphorylation and calcium levels after platelet ADP stimulation.

Phosphorylation data. We have extensive data on platelet protein interactions which we recently assembled to a systems biological database, the platelet knowledgebase PlateletWeb.[18] In particular, we have detailed information on site-specific phosphorylation of platelet proteins. The simulation data can hence be compared and validated by phosphorylation data stored in the database. In particular, the different phases postulated can be verified by checking which known experimental data validate involved individual phosphorylations.

The dynamical modelling allows us to predict the path in which the phosphorylations should occur. The different system states according to the platelet knowledgebase after mapping the dynamical simulation to the knowledgebase are given in Fig. 4 (high resolution pictures and references confirming interactions modelled in ESI,† part B). Furthermore, the knowledgebase allows us to zoom in on key nodes for each activation step and give all known experimental data for the surrounding interactome of this key node. For each activation step, we selected such key proteins and showed available phosphorylation information in the surrounding interactome. In phase 0 of the model, the platelet inhibited state is maintained by the PKA kinase. It phosphorylates a number of substrates depicted (Fig. 4A), which then ensure that the platelet will remain inactive. The phosphorylated targets are TBXA2R at S329[51] S330 and T332[52] and Rap1 at S180.[53] Phosphorylation of the two phosphodiesterases PDE5A[54] and PDE3A has also been confirmed in literature studies.[55] A well-established phosphorylation of the Src kinase at Y17 has been reported by a number of studies[56–59] and plays a role in Rap1 activation in NGF and cAMP signalling in PC12 cells.[60]

In phase 1 of the Boolean model two phosphorylated proteins have a change in their activatory state: Rap1A and Rap1B. The phosphorylation of Rap1B at S179 by PKA leads to cAMP inhibition of Akt kinase.[61] This phosphorylation site has also been reported earlier as a target of PKG1 kinase *in vitro*.[62] The phosphorylation of Rap1A at S180 by PKA modulates its interaction with other proteins and was measured *in vivo*.[63] The initial activation of the platelet by ADP signalling and the decrease of PKA mediated inhibition may also be contributed to the effect of decrease in phosphorylation of these sites on Rap1A and Rap1B. These small GTP-ases are crucial for the activation of integrins in platelets.[64]

The second phase of the model is associated with the activation of Akt1 and PKC kinase and the phosphorylation of Akt1 by PKC at S473 and T308 and PDE3A by PKC at S492, S428, S312, S438 and S465 which also has been shown previously.[65,66] The phosphorylation of S312 causes increased enzymatic activity of PDE3A. The third phase is characterized by a slight activation of the thromboxane receptor according to the model and its desensitization through phosphorylation by the strongly activated PKC kinase at T399 as reported.[67]

Activation of key-kinases. All types of prothrombotic outside-in signalling established in our model can exert their effect on integrin by means of two distinct ways: by engagement of CalDAG through mobilization of intracellular calcium pools, and recruitment of a sophisticated protein kinase network, which includes PKC, PI3-, Src- and Akt-kinase. Src thereby receives inputs of PKC and the inhibiting protein kinase A. In order to outweigh the taming effect of PKA on Src, PKC needs to be at least on level 2, otherwise Akt in turn will not exceed level 1, regardless of its other activator PI3-kinase. Table 2 gives an overview of the activation-states of the respective kinases and compares it to PlateletWeb data.[18]

Intracellular calcium. In our standard model scenario the system is excited by means of a combination of GPVI- and prostaglandin receptor-stimuli. Prostaglandins provoke *via* engagement of PKA the inhibition of IP3R. In the meantime, GPVI activates its own signalling-cascade and elicits the secretion of ADP and ATP. Paracrine ADP and ATP reach the plasma membrane with a short time-delay, bind to P2Y and P2X receptors and boost the intracellular calcium concentration as a result of calcium influx and PLC activation and subsequent IP_3 production. A second calcium increment is then mediated by the positive feedback loop involving SOCE.

For step-wise and stage-wise further functional validations, intracellular calcium concentration was detected after a combined stimulus of the prostanoid analogue iloprost and ADP (Fig. 5A). Starting with an iloprost input of 2 nM, calcium-levels first decrease as a result of PKA phosphorylation and thereby inhibiting the intracellular calcium-channel IP3R. Thus calcium-levels are abated slightly below the basal level of 500 arbitrary units. After 30 seconds ADP is added to the cells, and the calcium concentration increases to a value of 548. Due to retraction evoked by SERCA and PMCA as well as ion-exchanger-pumps (not included in the model), calcium levels drop to their basal levels. However, after 90 seconds store-operated-calcium-entry (SOCE) has to be considered. Thus the calcium concentration is increased again. The detected dynamics fit those of the simulated time course calculated with SQUAD (Fig. 3D).

The predicted behavior is thus supported by experimental measurements of intracellular calcium (Fig. 5A). The simulated ''peaking'' of calcium is robust against small GPVI-pulse level variations. However, it is only observed in a medium concentration range where the differences between slow and fast calcium channelling are well visible (as in the experimental data available, the effect vanishes at lower/higher concentrations in simulations and experimental measurements). The default scenario where the system is stimulated with an activating ligand alone was also tested experimentally, but could not directly be reproduced by SQUAD modeling. The data

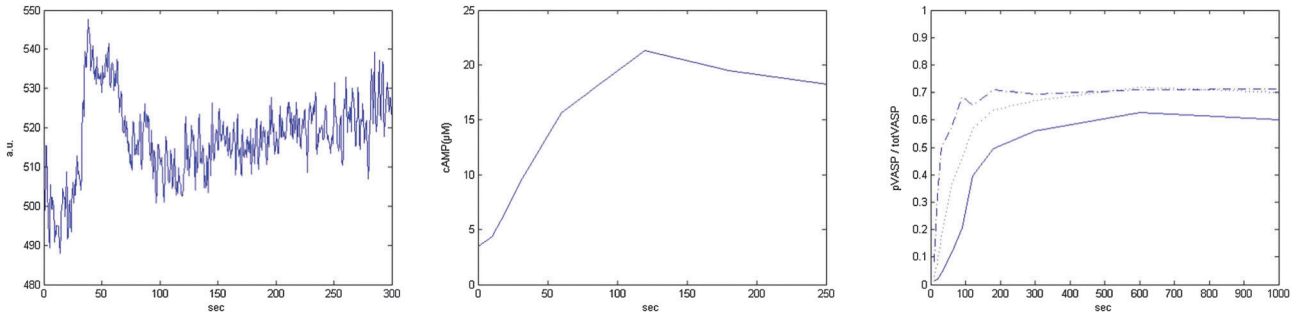

Fig. 5 (A–C) Validation. Measured time courses of key pathway components. Experimental measurements (see Materials and methods) confirm qualitatively predicted time courses. (A) Calcium measurement after iloprost stimulus (2 nM) at $t = 0$ combined with ADP stimulus (20 µM) at $t = 30$. (B) cAMP change after iloprost stimulus (2 nM). (C) VASP phosphorylation changes after stimulation at different concentrations of forskolin (solid = 5 µM, dotted = 20 µM, dash dotted = 100 µM).

showed a single peak followed by a continuing concentration decrease. Since in our model the fully activated state is stabilised by a positive feedback-loop, the system stays but active infinitely. It is an inherent SQUAD property to simulate as long as a steady-state condition is reached, which in this case is the activated state. Here, the semi-quantitative model is pushed to its limits.

Cyclic adenosine monophosphate (cAMP). cAMP is generated as a result of prostaglandin-evoked adenylyl cyclase activation. In a time-course-measurement, the abundance of intracellular cAMP was detected after stimulating the cells with 2 nM of iloprost (Fig. 5B). Following iloprost-stimulation, the concentration of cAMP forms a peak and is then steadily decreased, which is consistent with our model, where cAMP gets switched off in phase 1 due to the effect of PDE3.

The vasodilator stimulated phosphoprotein (VASP). VASP constitutes a target of protein kinase A and acts as an inhibitor of cytoskeletal rearrangements. In our model, it becomes phosphorylated at time point zero following an input through the prostanoid receptor and stays active until cAMP production is tempered through P2Y12 at time point 1. VASP phosphorylation (S239) is verified by a time-course measurement after stimulation with different concentrations of the allosteric adenylyl cyclase-activator forskolin (Fig. 5C). If cAMP production is not inhibited by means of ADP binding to P2Y12, the relative amount of phosphorylated VASP reaches a steady-state which stays constant for a period of 10–20 minutes (Fig. 5C).

In summary, validation of the different phases of activation suggested by the Boolean model is possible by different types of experimental data. This includes activation of involved kinases (Fig. 1), verification of phosphorylations for key nodes involved in the signalling cascade (Fig. 4A and B) as well as direct observations of cAMP levels under inhibitory regime as well as VASP phosphorylation and phase dependent changes of calcium levels under activatory conditions.

Applying the validated Boolean model, there are also predictions regarding pharmacological modulation or genetic mutations as well as an integrated view on platelet signalling with implications for different disease promoting system states possible.

Our model helps to understand system states of platelet activation. We distinguish four different phases, which are furthermore mirrored in different levels of calcium, cAMP and different strong phosphorylations in VASP as well as a detailed cascade of phosphorylation events in other proteins. Additionally, different inhibitory states are modelled. Subthreshold activation keeps the platelet below a committed reaction. We think this captures well the observed platelet behaviour, in particular that it integrates different inputs before finally, after threshold transgression, aggregation and secretion from platelets occur. Furthermore, both for better physiological description and for medical application our model shows that the fine tuned balance in platelet activation and inhibition relies on different positive and negative feedback loops as outlined above, which again could be validated by the available experimental data, can be monitored and allow pharmacological modulation. The PlateletWeb knowledgebase[18] gives furthermore information on drugs available to modulate involved key nodes (see ESI,† Table S3).

Clinical implications involve a better understanding of the pathology of the platelet including hyperreactive platelets or the inhibition by different antiplatelet drugs such as ticragrelor or abciximab (key interactions are marked in insets of Fig. 4A–D). The activation under or over threshold is an inherent feature of our model. It is again not only well compatible with all the experimental data collected here, but it may as well shed light on chronic inflammatory processes platelets are also involved in[68] since the above-mentioned feedback loops allow that in some platelets activation sustains the inflammatory process, while other keep inactivation. We think that this switching of states partly also mirrors system states of aging in the cardiovascular system: the population of the phases 0–3 in the platelet population is suggested to change with age of the patient, but maybe even more so with the age of the platelet. However, available experimental data are sparse and only future studies can validate this hypothesis.

Conclusion

We have successfully created a simplified Boolean model of the major signal transduction pathways present in platelets. Our model shows in a qualitative way the interaction of these

pathways and points out the most important events leading from first damaged tissue contact to irreversible aggregation and thrombus formation. We integrate cellular incidents like ADP secretion, liberation of calcium and complex phosphorylation patterns. These were previously analyzed in a disconnected manner. We model how all these components synergistically coalesce to accomplish the task of platelet activation, even under inhibiting environmental circumstances. Though the activation of the two output nodes, appointed as integrin function and cellular shape change, is due to the same processes, they still can be engaged independently to a certain degree. That means, even if particular network components are disrupted, the system is still able to respond to signals and to contribute to the objective of wound healing. Disruption of the GTPase Rap1, for instance, leads to platelet hyporeactivity: it prevents integrin from reaching its highest activation-level, however, as long as Akt phosphorylation and calcium mobilisation can occur, integrin is responsive to stimuli, the cytoskeleton can be rearranged and the platelet remains at least partially functional. Completed shape change and integrin activation leading to threshold transgression and irreversible aggregation are dependent on the full function of all signalling components, including calcium mobilisation, intact kinase network, positive feedback loop established by integrin outside-in signalling and both ADP and thromboxane secretion.

All in all our model can be used to demonstrate different states of platelet activation, examine inherent system properties like threshold behaviour and feedback loops, and serves to simulate versatile kinds of pathway disruptions like pharmacological interventions and genetically modified states. In combination with other models it may help to understand pathological processes in the cardiovascular and inflammatory system.

Due to the nature of the applied Boolean logic, complex reaction kinetics including collection of detailed and time resolved experimental data were neither considered nor required. Oscillating system behaviour can be observed for the continuous stimulatory input (see results above) but is neglected here in system state calculations (see Materials and methods), so that some potential for oscillations is detected in our simulations, but the model is here not fully realistic and not comprehensive. However, despite the approach's simplification, threshold analysis and pharmacological investigations allow interesting insights into the platelet's signal transduction network validated by experimental data, putting experimental observations and literature into their network and systems biology context. It represents an intermediate step on the way to an extensive ODE-based model of this medically highly relevant system.

Acknowledgements

This work was funded by the German Federal Ministry of Education and Research, Project SARA (FKZ 0315395B,C,E), DFG (GW,TD: SFB688-A2) and Land Bavaria (TD,MD).

References

1 R. Abbate, G. Cioni, I. Ricci, M. Miranda and A. M. Gori, *Thromb. Res.*, 2012, **129**(3), 235–240.
2 D. Lievens and P. von Hundelshausen, *Thromb. Haemostasis*, 2011, **106**(5), 827–838.
3 R. Scheppenheim, *Thromb. Res.*, 2011, **128**(Suppl. 1), S3–S7.
4 A. A. Weber, T. Hohlfeld and K. Schrör, *Platelets*, 1999, **10**(4), 238–241.
5 A. Singh, J. M. Nascimento, S. Kowar, H. Busch and M. Boerries, *Bioinformatics*, 2012, **28**(18), i495–i501.
6 J. E. Purvis, M. S. Chatterjee, L. F. Brass and S. L. Diamond, *Blood*, 2008, **112**(10), 4069–4079.
7 M. T. Walsh, J. F. Foley and B. T. Kinsella, *J. Biol. Chem.*, 2000, **275**(27), 20412–20423.
8 R. Schlatter, K. Schmich, I. Avalos Vizcarra, P. Scheurich, T. Sauter, C. Borner, M. T. Ederer, I. Merfort and O. Sawodny, *PLoS Comput. Biol.*, 2009, **5**(12), e1000595.
9 N. Philippi, D. Walter, R. Schlatter, K. Ferreira, M. Ederer, O. Sawodny, J. Timmer, C. Borner and T. Dandekar, *BMC Syst. Biol.*, 2009, **3**, 97.
10 R. Schlatter, N. Philippi, G. Wangorsch, R. Pick, O. Sawodny, C. Borner, J. Timmer, M. T. Ederer and T. Dandekar, *Briefings Bioinf.*, 2012, **13**(3), 365–376.
11 C. E. Shannon, *AIEE Trans.*, 1938, **57**, 471–495.
12 A. Singh, J. M. Nascimento, S. Kowar, H. Busch and M. Boerries, *Bioinformatics*, 2012, **28**(18), i495–i501.
13 J. Wollbold, R. Huber, D. Pohlers, D. Koczan, R. Guthke, R. W. Kinne and U. Gausmann, *BMC Syst. Biol.*, 2009, **3**, 77.
14 M. Cattaneo and C. Gachet, *Haematologica*, 2001, **86**(4), 346–348.
15 J. Geiger, P. Hönig-Liedl, P. Schanzenbächer and U. Walter, *Eur. J. Pharmacol.*, 1998, **351**, 235–246.
16 P. Savi, C. Labouret, N. Delesque, F. Guette, J. Lupker and J. M. Herbert, *Biochem. Biophys. Res. Commun.*, 2001, **283**(2), 379–388.
17 J. Liu, T. I. Pestina, M. C. Berndt, S. A. Steward, C. W. Jackson and T. K. Gartner, *J. Thromb. Haemostasis*, 2004, **2**(12), 2213–2222.
18 D. Boyanova, S. Nilla, I. Birschmann, T. Dandekar and M. Dittrich, *Blood*, 2012, **119**(3), e22–e34.
19 M. Billah, E. G. Lapetina and P. Cuatrecasas, *J. Biol. Chem.*, 1980, **255**(21), 10227–10231.
20 S. E. Rittenhouse and J. P. Sasson, *Nouv. Rev. Fr. Hematol.*, 1985, **27**(4), 239–242.
21 R. I. Kirk, M. R. Sanderson and K. M. Lerea, *J. Biol. Chem.*, 2000, **275**(40), 30901–30906.
22 A. Smolenski, *J. Thromb. Haemostasis*, 2012, **10**(2), 167–176.
23 H. Abrahamsen, T. Vang and K. Taskén, *J. Biol. Chem.*, 2003, **278**(19), 17170–17177.
24 K. S. Murthy and H. Zhou, *Am. J. Physiol.: Gastrointest. Liver Physiol.*, 2003, **284**(2), G221–G230.
25 A. A. Weber, T. Hohlfeld and K. Schrör, *Platelets*, 1999, **10**(4), 238–241.

26 M. A. Feijge, K. Ansink, K. Vanschoonbeek and J. W. Heemskerk, *Biochem. Pharmacol.*, 2004, **67**(8), 1559–1567.
27 J. Geiger, T. Brandmann, K. Hubertus, B. Tjahjadi, R. Schinzel and U. Walter, *Anal. Biochem.*, 2010, **407**(2), 261–269.
28 J. Liu, T. I. Pestina, M. C. Berndt, S. A. Steward, C. W. Jackson and T. K. Gartner, *J. Thromb. Haemostasis*, 2004, **2**(12), 2213–2222.
29 A. Braun, D. Varga-Szabo, C. Kleinschnitz, I. Pleines and M. Bender, *Blood*, 2009, **113**(9), 2056–2063.
30 M. P. Mahaut-Smith, S. Jones and R. J. Evans, *Purinergic Signalling*, 2011, **7**(3), 341–356.
31 S. Klamt, J. Saez-Rodriguez and E. D. Gilles, *BMC Syst. Biol.*, 2007, **1**, 2.
32 S. Klamt, J. Saez-Rodriguez, J. A. Lindquist, L. Simeoni and E. D. Gilles, *BMC Bioinf.*, 2006, **7**, 56.
33 A. Di Cara, A. Garg, G. De Micheli, I. Xenarios and L. Mendoza, *BMC Bioinf.*, 2007, **8**, 462.
34 J. Geiger, P. Hönig-Liedl, P. Schanzenbächer and U. Walter, *Eur. J. Pharmacol.*, 1998, **351**, 235–246.
35 E. G. Lapetina, B. Reep, B. R. Ganong and R. M. Bell, *J. Biol. Chem.*, 1985, **260**(3), 1358–1361.
36 K. S. Authi and N. Crawford, *Biochem. J.*, 1985, **230**(1), 247–253.
37 J. R. Crittenden, W. Bergmeier, Y. Zhang, C. L. Piffath, Y. Liang, D. D. Wagner, D. E. Housman and A. M. Graybiel, *Nat. Med.*, 2004, **10**(9), 982–986.
38 U. Liebenhoff and A. Greinacher, *Cell Mol. Biol.*, 1994, **40**(5), 645–652.
39 K. S. Murthy and H. Zhou, *Am. J. Physiol.*, 2003, **284**(2), G221–G230.
40 B. Xiang and G. Zhang, *J. Thromb. Haemostasis*, 2010, **8**(9), 2032–2041.
41 R. I. Kirk, M. R. Sanderson and K. M. Lerea, *J. Biol. Chem.*, 2000, **275**(40), 30901–30906.
42 M. Cattaneo, M. T. Canciani, A. Lecchi, R. L. Kinlough-Rathbone, M. A. Packham, P. M. Mannucci and J. F. Mustard, *Blood*, 1990, **75**(5), 1081–1086.
43 M. Cattaneo and C. Gachet, *Haematologica*, 2001, **86**(4), 346–348.
44 G. Wangorsch, E. Butt, R. Mark, K. Hubertus, J. Geiger, T. Dandekar and M. Dittrich, *BMC Syst. Biol.*, 2011, **5**, 17.
45 R. L. Jones, D. F. Woodward, J. W. Wang and R. L. Clark, *Br. J. Pharmacol.*, 2011, **162**(4), 863–879.
46 S. Grüner, M. Prostredna, M. Koch, Y. Miura, V. Schulte, S. M. Jung, M. Moroi and B. Nieswandt, *Blood*, 2005, **105**(4), 1492–1499.
47 Y. Li, B. C. Tai, W. Sia, Q. H. Phua, M. A. Richards, A. Low, K. H. Chan, S. G. Teo, T. B. Sim, C. H. Lee, M. T. Roe, T. C. Yeo, H. C. Tan and M. Y. Chan, *J. Thromb. Thrombolysis*, 2012, **34**(4), 499–505.
48 H. Haberstock-Debic, P. Andre, S. Mills, D. R. Phillips and P. B. Conley, *J. Pharmacol. Exp. Ther.*, 2011, **339**(1), 54–61.
49 D. Iyú, J. R. Glenn, A. E. White, S. C. Fox, N. Dovlatova and S. Heptinstall, *Platelets*, 2011, **22**(7), 504–515.
50 R. L. Jones, D. F. Woodward, J. W. Wang and R. L. Clark, *Br. J. Pharmacol.*, 2011, **162**(4), 863–879.
51 M. T. Walsh, J. F. Foley and B. T. Kinsella, *J. Biol. Chem.*, 2000, **275**(27), 20412–20423.
52 P. V. Hornbeck, I. Chabra, J. M. Kornhauser, E. Skrzypek and B. Zhang, *Proteomics*, 2004, **4**(6), 1551–1561.
53 C. D. Hu and K. Kariya, *J. Biol. Chem.*, 1999, **274**(1), 48–51.
54 M. K. Thomas, S. H. Francis and J. D. Corbin, *J. Biol. Chem.*, 1990, **265**(25), 14971–14978.
55 M. Pozuelo Rubi, D. G. Campbell, N. A. Morrice and C. Mackintosh, *Biochem. J.*, 2005, **392**, 163–172.
56 L. M. Brill, W. Xiong, K. B. Lee, S. B. Ficarro, A. Crain, Y. Xu, A. Terskikh, E. Y. Snyder and S. Ding, *Cell Stem Cell*, 2009, **5**(2), 204–213.
57 G. Han and M. Ye, *Electrophoresis*, 2010, **31**(6), 1080–1089.
58 C. Pan, J. V. Olsen, H. Daub and M. Mann, *Mol. Cell. Proteomics*, 2009, **8**(12), 2796–2808.
59 R. Zahedi, U. Lewandrowski, J. Wiesner, S. Wortelkamp, J. Moebius and C. Schütz, *J. Proteome Res.*, 2008, **7**(2), 526–534.
60 Y. Obara, K. Labudda, T. J. Dillon and P. J. Stork, *J. Cell Sci.*, 2004, **117**(Pt 25), 6085–6094.
61 L. Lou, J. Urbani, F. Ribeiro-Neto and D. L. Altschuler, *J. Biol. Chem.*, 2002, **277**(36), 32799–32806.
62 Y. Miura, K. Kaibuchi, T. Itoh, J. D. Corbin, S. H. Francis and Y. Takai, *FEBS Lett.*, 1992, **297**(1–2), 171–174.
63 C. D. Hu and K. Kariya, *J. Biol. Chem.*, 1999, **274**(1), 48–51.
64 A. Banno and M. H. Ginsberg, *Biochem. Soc. Trans.*, 2008, **36**(Pt 2), 229–234.
65 R. W. Hunter, C. Mackintosh and I. Hers, *J. Biol. Chem.*, 2009, **284**(18), 12339–12348.
66 C. Kroner, K. Eybrechts and J. W. Akkerman, *J. Biol. Chem.*, 2000, **275**(36), 27790–27798.
67 L. P. Kelley-Hickie and B. T. Kinsella, *Br. J. Pharmacol.*, 2004, **142**(1), 203–221.
68 M. Leslie, *Science*, 2010, **328**(5978), 562–564.
69 A. Karniguian, F. Grelac, S. Levy-Toledano, Y. J. Legrand and F. Rendu, *Biochem. J.*, 1990, **268**(2), 325–331.
70 M. F. Hoylaerts, C. Oury, E. Toth-Zsamboki and J. Vermylen, *Platelets*, 2000, **11**(6), 307–309.
71 A. D. Kohn, F. Takeuchi and R. A. Roth, *J. Biol. Chem.*, 1996, **271**(36), 21920–21926.
72 B. Hechler, C. Léon, C. Vial, P. Vigne, C. Frelin, J. P. Cazenave and C. Gachet, *Blood*, 1998, **92**(1), 152–159.
73 N. Watanabe, L. Bodin, M. Pandey, M. Krause, S. Coughlin, V. A. Boussiotis, M. H. Ginsberg and S. J. Shattil, *J. Cell Biol.*, 2008, **181**(7), 1211–1222.
74 M. G. Rolf and M. P. Mahaut-Smith, *Thromb. Haemostasis*, 2002, **88**(3), 495–502.
75 J. L. Daniel, C. Dangelmaier, J. Jin, Y. B. Kim and S. P. Kunapuli, *Thromb. Haemostasis*, 1999, **82**(4), 1322–1326.
76 P. K. Forsell, A. O. Olsson, E. Andersson, L. Nallan and M. H. Gelb, *Biochem. Pharmacol.*, 2005, **71**(1–2), 144–155.

77 J. Balsinde, M. A. Balboa and E. A. Dennis, *Proc. Natl. Acad. Sci. U. S. A.*, 1998, **95**(14), 7951–7956.
78 P. C. Kam and A. U. See, *Anaesthesia*, 2000, **55**(5), 442–449.
79 N. Nakahata, *Pharmacol. Ther.*, 2008, **118**(1), 18–35.
80 Y. Suzuki, M. Yamamoto, H. Wada, M. Ito, T. Nakano, Y. Sasaki, S. Narumiya, H. Shiku and M. Nishikawa, *Blood*, 1999, **93**(10), 3408–3417.
81 A. Ishii-Watabe, E. Uchida, H. Mizuguchi and T. Hayakawa, *Life Sci.*, 2001, **69**(8), 945–960.
82 B. G. Petrich, P. Marchese, Z. M. Ruggeri, S. Spiess, R. A. Weichert, F. Ye, R. Tiedt, R. C. Skoda, S. J. Monkley, D. R. Critchley and M. H. Ginsberg, *J. Exp. Med.*, 2007, **204**(13), 3103–3111.
83 R. A. Armstrong, *Pharmacol. Ther.*, 1996, **72**(3), 171–191.
84 T. H. Fischer and G. C. White, *Biochem. Biophys. Res. Commun.*, 1987, **149**(2), 700–706.
85 W. Siess, D. A. Winegar and E. G. Lapetina, *Biochem. Biophys. Res. Commun.*, 1990, **170**(2), 944–950.
86 J. Qiao, O. Holian, B. S. Lee, F. Huang, J. Zhang and H. Lum, *Am. J. Physiol.: Cell Physiol.*, 2008, **295**(5), C1161–C1168.
87 J. Jin, T. M. Quinton, J. Zhang, S. E. Rittenhouse and S. P. Kunapuli, *Blood*, 2002, **99**(1), 193–198.